Eur. Phys. J. B **22**, 157–165 (2001)

THE EUROPEAN PHYSICAL JOURNAL B

EDP Sciences

Jahn-Teller, charge and magnetic ordering in half-doped manganese oxides

S. Fratini[1], D. Feinberg[2,a], and M. Grilli[1]

[1] Istituto Nazionale di Fisica della Materia and Dipartimento di Fisica, Università di Roma "La Sapienza", Piazzale Aldo Moro 2, 00185 Roma, Italy
[2] Laboratoire d'Études des Propriétés Électroniques des Solides, Centre National de la Recherche Scientifique, associated with Université Joseph Fourier, BP 166, 38042 Grenoble Cedex 9, France

Received 28 November 2000

Abstract. The phase diagram of half-doped manganite systems of formula $A_{0.5}A'_{0.5}MnO_3$ is investigated within a single-orbital model incorporating magnetic double-exchange and superexchange, together with intersite Coulomb and electron-lattice interactions. Strong Jahn-Teller and breathing mode deformations compete together and result in shear lattice deformations. The latter stabilize the charge-ordered CE-type phase, which undergo first-order transitions with temperature or magnetic field to either Ferromagnetic metallic or Paramagnetic insulating phases. An essential feature is the self-consistent screening of Coulomb and electron-phonon interactions in the ferromagnetic phase.

PACS. 75.30.-m Intrinsic properties of magnetically ordered materials – 75.30.Vn Colossal magnetoresistance – 63.20.Kr Phonon-electron and phonon-phonon interactions

Manganese perovskite oxides are currently the object of intense activity. Motivated initially by the colossal magnetoresistance phenomena, more recent studies have revealed an extremely rich phase diagram originating from the interplay of charge, lattice, orbital and magnetic degrees of freedom [1]. The general formula is $A_{1-x}A'_xMnO_3$ where A is in general a trivalent rare earth element (La, Pr, Nd) and A′ a divalent alcaline element (Sr, Ca). Substitutional doping allows to explore the full phase diagram, from $x = 0$ to $x = 1$. At the extremes, $LaMnO_3$ and $CaMnO_3$ are antiferromagnetic insulators. The former is a layered antiferromagnet, which can be explained thanks to the large Jahn-Teller couplings of the e_g electrons of Mn^{3+} ions [2]. The latter shows a Néel ordering due to antiferromagnetic exchange of t_{2g} electrons [3]. With doping, the double-exchange phenomena originating from Hund's coupling between e_g and t_{2g} electron spins can stabilize a metallic ferromagnetic phase [4–6]: Coherent band motion occurs for ferromagnetic ordering, while strong inelastic scattering takes place in the high temperature paramagnetic phase. Very large magnetoresistance is obtained when the applied magnetic field is able to align t_{2g} spins, thereby favouring the metallic phase. Nevertheless, it has been pointed out that spin scattering alone is not sufficient to quantitatively explain the phenomenon. Millis *et al.* [7] suggested that a large electron-lattice coupling is involved, with the formation of Jahn-Teller polarons in the insulating phase. Such large couplings are quite expected from the very large cooperative Jahn-Teller distortions existing in $LaMnO_3$. Those deformations indeed involve more than ten per cent variations of the Mn-O bond lengths around all Mn^{3+} ions. Local deformations have been indeed revealed in charge-disordered phases by X-ray and neutron spectroscopy, as well as optical measurements. They consist of Jahn-Teller deformations around Mn^{3+} ions, and "breathing mode" deformations with shorter Mn-O bonds around Mn^{4+} ions. The role of these deformations becomes more stringent in the charge-ordered phases (CO) of doped manganites. These phases strongly compete with the ferromagnetic metallic (FM) one at sufficient doping. Besides the Coulomb interaction between electrons on Mn ions, electron-phonon interaction should play a prominent role in this phenomenon. This is exemplified by the nature of charge ordering at half-doping, for instance in $La_{0.5}Ca_{0.5}MnO_3$: While Mn^{3+} and Mn^{4+} ions alternate in two directions (say, a and b), in the other direction (which we here define as the c-axis), one finds rows of Mn^{3+} or Mn^{4+} ions. If CO were exclusively due to intersite Coulomb interaction, one would on the contrary expect a Wigner crystal ordering, alternated in all directions. This shows that cooperative lattice distortions are an essential ingredient to understand charge ordering [8].

Charge ordering at $x = 0.5$ is accompanied by CE-type antiferromagnetic order: In the ab directions,

[a] e-mail: feinberg@lepes.polycnrs-gre.fr

it involves ferromagnetic and antiferromagnetic zigzag chains crossing each other. A qualitative explanation was given a long time ago by Goodenough [9], following the pioneering structural analysis of Wollan and Koehler [3]: The cooperative Jahn-Teller distortions are accompanied by orbital ordering, and induce the magnetic structure. Moreover, away from half-doping, this CE structure appears as an elementary "brick" to build more complicated charge ordering patterns such as "stripes" [10]. It is thus especially robust and calls for a detailed explanation.

A few models have been proposed to explain CE ordering, putting the emphasis either on intersite Coulomb interactions [11], magnetism and orbital ordering [12,13]. Mizokawa *et al.* [14], and Yunoki and coworkers [8] have underlined the prominent role of Jahn-Teller deformations.

Let us first list and grossly estimate the various energy scales in the system. The on-site Hubbard repulsion U and the atomic level difference between the e_g orbitals of manganese and the $2p$ orbitals of the oxygen are of the order of several eV's, and are larger than the total conduction bandwidth ($W \sim 3$ eV). The Hund coupling $J_{\rm H}$ is of order 1 eV, while the intersite Coulomb repulsion seems not to be larger than 0.5 eV. The Jahn-Teller splitting in the insulating $LaMnO_3$ phase is comparable, as shown by spectroscopy and optical absorption measurements [15,16]. In terms of a local electron-phonon coupling, it is reasonable to think of energies of the order of 0.2–0.3 eV, comparable to the intersite e_g hopping integrals $t_0 \sim 0.1-0.4$ eV depending on the d-orbitals involved. On the other hand, the magnetic couplings (which in a cubic lattice give rise to critical temperatures $T_{\rm c}$ between 100 K and 400 K) are in the range of a few meV. This holds as well for the superexchange (antiferromagnetic) couplings as, more surprisingly, for the (ferromagnetic) double-exchange ones. It has been shown by Zener [4] that $T_{\rm c}^{\rm DE} \sim \alpha t_0$, *e.g.* is proportional to the total kinetic energy of the carriers. As will be shown below, α is quite small and the actual values of $T_{\rm c}^{\rm DE}$ can be easily explained with a realistic t_0, for instance within De Gennes's mean-field picture [6]. This hierarchy of energy scales is completed by the one set by the external magnetic field needed to turn the FM phase into the CE (AFCO) phase: It ranges from a few teslas to 20 teslas or more. In terms of energy scale per atom, this is very small, of the order of 0.4–4 meV. It is thus consistent with the values of the magnetic exchange constants, but much smaller than all the other scales. This points towards an important conclusion: The stringent competition between the above phases require that their free energies be very close, in the range of a few meV per atom. Owing to the much larger electron-phonon and Coulomb interactions, it is reasonable to suppose that they play a dominant role in stabilizing the low-temperature CE phase. The necessary conclusion is that CE and FM phases are (meta)stable minima of the free energy, separated by rather high barriers. This is consistent with the fact that the phase transitions (with temperature or magnetic field) between charge ordered and charge disordered phases are first-order, with strong hysteresis under magnetic field. Tendencies to phase separation between FM and CO phases have been demonstrated in $La_{0.5}Ca_{0.5}MnO_3$, $Pr_{0.7}Sr_{0.3}MnO_3$ and other compositions. One should also notice that charge ordering is always strong when it exists. Fine tuning of the chemical composition between CO and FM low temperature phases [17] does not allow to stabilize "weak" charge ordering. This points towards strong interactions (electron-phonon or Coulomb) in the insulating phase, while they are screened in the metallic phase. This feature is overlooked by mean-field treatments, but can be recovered by taking into account exchange-correlation corrections to the intersite Coulomb repulsion, as shown by Sheng and Ting [18]. Since the lattice distortions here also come from Coulomb interactions (between Mn and O ions), we propose here to generalize the screening idea to electron-phonon interactions and use for this purpose a phenomenological approach.

Given the complexity of the overall Hamiltonian, here we restrict ourselves to a single-orbital model in two dimensions, which quantitatively reproduces the various phase diagrams and their tuning by subtle variations of the bandwidth. Our goals are i) obtaining, for realistic values of the parameters, FM, CE and paramagnetic phases; ii) exploring by small variations of those parameters the different kinds of phase diagrams, with temperature and magnetic field: Of the type of $La_{0.5}Sr_{0.5}MnO_3$ (no charge ordering, FM-PM transition with increasing T); of the type of $Nd_{0.5}Sr_{0.5}MnO_3$ (CE-FM-PM transitions with T, CE-FM with H); of the type of $Pr_{0.5}Ca_{0.5}MnO_3$ (CE-PMCO-PM transitions with T, CE-FM with H); iii) obtaining first-order transitions between CE and FM phases.

Taking into account explicitly orbital ordering should not change qualitatively the results since it works in the same direction [8,13] but may lead to quantitative improvement.

1 Model and approximations

1.1 Hamiltonian

According to the arguments given in the introduction, we assume an infinite repulsion ($U = \infty$) between electrons on the same lattice site, and an infinite Hund coupling ($J_{\rm H} = \infty$) between the localized t_{2g} spins and the itinerant e_g spins. One can therefore consider spinless electrons, their spin degree of freedom being unequivocally defined by the direction of the local t_{2g} spins $\mathbf{S}$. Furthermore, we consider in this work a two-dimensional plane of the structure, with a half-filled band made of a single e_g orbital. The effective model Hamiltonian is then:

$$H = H_{\rm DE} + H_{\rm Coul} + H_{\rm ph} + H_{\rm SE} + H_{\rm H} \qquad (1)$$

with

$$H_{\rm DE} = -\sum_{\langle ij\rangle} \tilde{t}_{ij} c_i^\dagger c_j$$

$$H_{\rm Coul} = \sum_{\langle ij\rangle} V(n_i - n)(n_j - n)$$

$$H_{\rm ph} = \frac{1}{2}\sum_i [K_b Q_{bi}^2 + K_2 Q_{2i}^2 + K_s Q_{si}^2]$$

$$- \sum_i g_2 Q_{2i}(n_i - n) + \sum_i g_b Q_{bi}(n_i - n) - L_s \sum_{\langle ij\rangle} Q_{si} Q_{2j}$$

$$H_{\rm SE} = \sum_{\langle ij\rangle} [J_1 - J_2 Q_s] \mathbf{S}_i \cdot \mathbf{S}_j$$

$$H_{\rm H} = -g\mu_b \boldsymbol{H} \sum_i \mathbf{S}_i.$$

The first term $H_{\rm DE}$ represents the double exchange hopping of electrons on a square lattice. Here $c_i^\dagger$, c_i are respectively the creation and annihilation operators for spinless electrons from a single band, and $\tilde{t}_{ij} = t\cos(\theta_{ij}/2)$ is the transfer integral between neighboring Mn sites whose ionic spins $\mathbf{S}_i$ and $\mathbf{S}_j$ make an angle θ_{ij} [5].

The second term $H_{\rm Coul}$ describes the Coulomb repulsion between nearest neighbors ($n_i = c_i^\dagger c_i$ and n is the average electron density, which is equal to $1/2$ in the present case).

The third term $H_{\rm ph}$ is the elastic part, which includes the coupling of electrons to a Jahn-Teller (JT) mode Q_2 and of holes to a "breathing" mode Q_b (g_2 and g_b are the coupling strengths, K_2 and K_b the spring constants). In the planar geometry considered here, the other Jahn-Teller mode Q_1 is not relevant. We have also introduced a shear mode Q_s, which is driven by Q_2. Such a shear deformation, which is experimentally observed at low temperatures, is essential to reconcile the alternating Mn^{4+} breathing and Mn^{3+} JT distortions which develop in the ordered phases. A substantial shear deformation is indeed observed in $La_{0.5}Ca_{0.5}MnO_3$ [19]. It results in some Mn-O-Mn bonds being shorter and other larger ("zig-zag" chains, see Fig. 1).

The term $H_{\rm SE}$ represents the antiferromagnetic (AF) superexchange interaction J_1 between the ionic spins on neighboring sites, which are treated as classical. The additional term $J_2 Q_s$ is a phenomenological implementation of the Goodenough rule: It can either enhance or reduce the AF coupling depending on the sign of the shear deformation, which accounts for the fact that longer (shorter) Mn-Mn bonds have a more (less) antiferromagnetic character [9]. The last term $H_{\rm H}$ takes into account the external magnetic field.

We shall study the Hamiltonian (1) in the mean-field approximation, describing the charge ordered (CO) phase as a charge density wave (CDW) with momentum (π, π). Let us call $\bar{n}^A$ and $\bar{n}^B$ the average electron densities in the two resulting sublattices, which correspond respectively to the Mn^{3+} and Mn^{4+} ions. We shall further assume that the JT coupling is only active on A sites, while the breathing deformations arise on B sites. With these approximations, the terms in the Hamiltonian which depend explicitely on $(n_i - n)$ reduce to

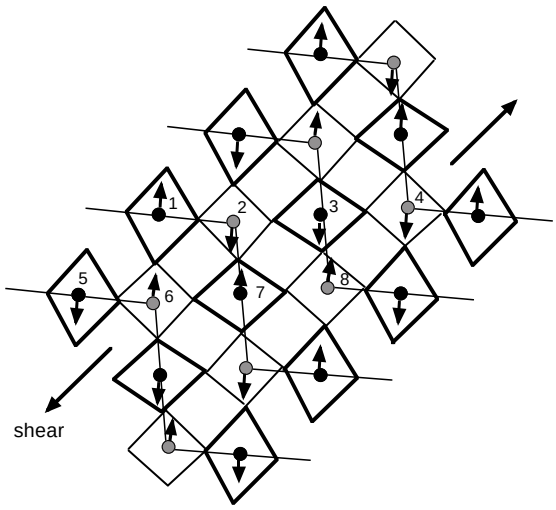

Fig. 1. The CE structure and the unit cell (ions 1 to 8) in the *ab* plane: Mn^{3+} Jahn-Teller ions (black circles) are at the center of distorted Mn-O rhombus, and Mn^{4+} ions (grey circles) undergo shear displacements, forming zig-zag chains with short (antiferromagnetic) and long (ferromagnetic) bonds.

$$H_{\rm MF} = -\Delta \sum_{i\in A or B} (n_i^A - n_i^B) + \text{const.}, \qquad (2)$$

where the order parameter Δ is defined as

$$\Delta = 2V(\bar{n}^A - \bar{n}^B) + (g_b Q_b + g_2 Q_2)/2 \qquad (3)$$

and the chemical potential has been set to zero by adding a term $\Delta\mu = -(g_2 Q_2 - g_b Q_b)/2$ to recover particle-hole symmetry (with these notations, the choice $\bar{n}^A \geq \bar{n}^B$ corresponds to the Q's being all positive).

The magnetic part is also treated in mean-field, according to de Gennes' procedure [6], using a Gaussian distribution for the angle of the classical spins with respect to the mean field direction. We consider the following magnetic phases: Ferromagnetic (F), paramagnetic (P), Néel anti-ferromagnetic (NAF), and CE-type ordering, with ferromagnetic zig-zag chains, coupled anti-ferromagnetically (CE). The most general unit cell which allows to describe all these phases is is made of 8 nonequivalent Mn sites in a plane (Fig. 1). In each of these magnetic configurations, the total free energy is minimized with respect to the following parameters: i) the magnetization on nonequivalent magnetic sites, ii) the average electron density $\bar{n}^A$ on sublattice A ($\bar{n}^B$ being just $1 - \bar{n}^A$) and iii) the lattice displacements.

1.2 Phenomenological treatment of screening effects

As mentioned in the Introduction, to have a realistic description of the phase diagram which includes both the metallic and charge ordered phases at half-filling, it is

necessary to go beyond the simple mean-field approach described in the preceding section by including the effects of exchange and correlation. Such effects on the intersite Coulomb repulsion in the half-doping manganites have recently been analyzed within an RPA-like calculation [18], which is known to be appropriate for interacting electron systems at metallic densities. Since a detailed study goes beyond the scope of this paper, we propose here a semi-phenomenological treatment of screening which allows a qualitative description of the transition between CO and metallic states, and which correctly reproduces the results of reference [18]. The method is further generalized to describe the screening of the electron-lattice interactions. Actually, the latter are due to the Coulomb repulsion between Mn and O ions and are therefore also screened in the metallic phase. This screening should be weaker than that of Mn-Mn interactions, since it involves Mn-O rather than Mn-Mn charge fluctuations, but it should be sizeable.

The procedure will be carried out in two successive steps. The first step consists in writing a reasonable estimate for the exchange-correlation energy $E_{\rm xc}$, which is defined as the correction to the ground-state energy beyond the Hartree mean-field result. In the second step, we shall define an effective Hamiltonian $H_{\rm xc}$ to be treated in the mean-field approximation, such that

$$\langle H_{\rm xc}\rangle = E_{\rm xc}. \tag{4}$$

This results in a modification of the atomic energy levels $\pm\Delta$ (*i.e.* in a reduction of the CDW gap), and it yields a correction to the free energy which is precisely of the form $E_{\rm xc}$.

1.2.1 Exchange-correlation energy

Exchange-correlation corrections to the mean-field analysis have been calculated by Sheng and Ting in the Random Phase Approximation (RPA), for a double exchange model including Coulomb interactions [18]. Let us discuss the ferromagnetic case at $T = 0$, where the electron hopping is not renormalized by the mechanism of double exchange. First, in the metallic phase, which corresponds to a vanishing order parameter Δ, the leading correction appears to be nearly proportional to the interaction potential V, and one can write $E_{\rm xc} \sim -aV$. On the other hand, in the CO phase, *i.e.* at strong Δ, the correlation energy corresponds to the interaction between density fluctuations on neighboring sites, each of them being proportional to $\delta n \sim t/\Delta$. Therefore, in this case the appropriate limiting formula is $E_{\rm xc} \sim -V(t/\Delta)^2$. This is actually what is found by Sheng and Ting. The RPA calculation between these two limits leads to the typical first-order behaviour [18]: a free energy minimum exists at zero gap, and the system passes abruptly from $\Delta = 0$ to a large Δ at a critical value of the interaction parameter V. Since in the strong coupling regime the V term and the lattice-mediated interaction g^2/K play a similar role (*e.g.* in driving a charge-ordered state), we propose that the result for the screening of V can be generalized to the screening of the electron-lattice interactions, by replacing $V \to g^2/K$ and by introducing the corresponding order parameter Δ as given by equation (3). A smooth interpolation between the weak and strong coupling behaviors can be obtained by writing the following expression for the exchange-correlation energy:

$$E_{\rm xc} = -\frac{aV + b(g_b^2/K_b + g_2^2/K_2)}{1 + c\left(\frac{\Delta}{t}\right)^2} \tag{5}$$

where a, b and c are phenomenological parameters (the ratio $a/c = 1.44$ can be deduced from reference [18] and $b/a = 1/10$ is chosen according to the ionic distances).

As was stated at the beginning of this section, this formula is only appropriate in the ferromagnetic case. It does not account for the fact that the mobility of the carriers taking part in the screening process is affected by the magnetic structure through the DE mechanism. We shall give here the arguments which allow a generalization of equation (5) to the different kinds of magnetic orderings.

In the free-electron limit ($\Delta \to 0$), where screening is due to coherent band motion, one expects the correlation energy to be reduced by a factor $\tilde{t}/t$, where

$$\tilde{t} = t\langle\cos(\theta_{ij}/2)\rangle \tag{6}$$

is the effective DE hopping parameter averaged in all space directions (this gives respectively $1, 8/9, 1/2$ in the F, P, CE phases). The situation is slightly more complicated in the charge ordered phases, because $E_{\rm xc}$ comes from incoherent hopping of the carriers to neighboring sites. According to Hund's rule, such processes will be allowed only between sites with parallel spins, which defines an effective number of neighbors $\tilde{z} \leq z$.

In the CE phase, for instance, the lattice can be divided into U (up) and D (down) sites, according to the spin direction. Since each site has 2 U and 2 D neighbors, a given electron can only hop to the 2 neighbors with the same spin direction, and consequently $\tilde{z}/z = 1/2$. At finite temperatures, however, thermal fluctuations will reduce the absolute value of the local magnetization m. Accordingly, there will be a finite probability that a given U site has a $\downarrow$ spin, which is given by $n_U^{\downarrow} = (1 - m_U)/2$ (an equivalent expression holds for D sites). The total probability for hopping away from a U site is therefore

$$2n_U^{\uparrow}n_U^{\uparrow} + 2n_U^{\downarrow}n_U^{\downarrow} + 2n_U^{\uparrow}n_D^{\uparrow} + 2n_U^{\downarrow}n_D^{\downarrow}$$

where obviously $n_U^{\uparrow} = 1 - n_U^{\downarrow}$. By adding the contributions for hopping processes starting from both U and D sites and dividing by 2, we obtain

$$\tilde{z} = \frac{1}{2}\left[4 + (m_U + m_D)^2\right] \tag{7}$$

which correctly gives $\tilde{z}/z = 1, 1/2, 1/2$ for the F,P,CE phases at $T = 0$. Here the factors (6) and (7) introduce a feedback on the itinerancy of the electrons in the case of an applied magnetic field, which tends to align the spins ferromagnetically. This effect is essential in reducing the critical H for the CE-FM transition at low temperatures, as we shall see below.

For each given magnetic configuration, instead of equation (5), we shall use the following formula for the exchange-correlation energy:

$$\tilde{E}_{\rm xc} = -\frac{\left[\tilde{a}V + \tilde{b}(g_b^2/K_b + g_2^2/K_2)\right]}{1+\tilde{c}\left(\frac{\Delta}{t}\right)^2} \qquad (8)$$

where the screening parameters a, b, c have been modified according to

$$\tilde{a} = a\frac{\tilde{t}}{t}, \qquad \tilde{b} = b\frac{\tilde{t}}{t}, \qquad \tilde{c} = c\frac{z}{\tilde{z}}\frac{\tilde{t}}{t}\cdot \qquad (9)$$

We emphasize here that the terms in the numerator of equation (5) are rescaled by the $\tilde{t}/t$ factor since they arise from the coherent screening processes (mostly active when $\Delta \to 0$). On the other hand the local (incoherent) screening processes related to the term in the denominator of equation (5) are also rescaled by the effective number of accessible nearest neighbor sites.

1.2.2 Mean-field potential from exchange and correlation

We wish to define an effective Hamiltonian $H_{\rm xc}$ to be treated in the mean-field approximation such that the correction to the free energy is equal to $E_{\rm xc}$. To this purpose, we replace Δ by an operator $\hat{\Delta}$ (*e.g.* the mean-field parameter n^A is replaced by $\sum_{i\in A} n_i^A$), and linearize the resulting expression. This gives

$$H_{\rm xc} = B\tilde{c}\frac{V}{t}\frac{\Delta}{t}\sum_{i\in A or B}(n_i^A - n_i^B) + \text{const.}, \qquad (10)$$

where we have defined

$$B = \left[\tilde{a}V + \tilde{b}(g_b^2/K_b + g_2^2/K_2)\right] / \left[1+\tilde{c}\left(\frac{\Delta}{t}\right)^2\right]^2 \cdot \qquad (11)$$

The constant part in equation (10) is

$$-B\left\{1+\tilde{c}\frac{\Delta}{t^2}\left[6V(\bar{n}^A - \bar{n}^B) + (g_bQ_b + g_2Q_2)/2\right]\right\}\cdot \qquad (12)$$

It is easy to verify that equation (4) holds when $\bar{n}^A = \langle n^A\rangle$ and $\bar{n}^B = \langle n^B\rangle$.

One notices that a dielectric constant can be deduced from the screening of the gap, by writing

$$\Delta \to \Delta_{\rm eff} = \Delta - B\tilde{c}\frac{V\Delta}{t^2}$$

which gives

$$\varepsilon = \frac{\Delta}{\Delta_{\rm eff}} = \frac{1}{1 - c\frac{V}{t^2}\frac{\tilde{a}V+\tilde{b}(g_b^2/K_b+g_2^2/K_2)}{1+\tilde{c}\left(\frac{\Delta}{t}\right)^2}}.$$

2 Results

2.1 The phase diagram: Existence of a CE phase

The Hamiltonian in equation (1) is formed by several competing terms, and the corresponding phase diagram contains several phases, each one dominating in some region of the parameter space. To make the analysis simpler, we choose to vary together those parameters having similar physical effects. In particular, the electron-phonon couplings generically reduce the electron mobility and, at mean-field level, tend to give rise to a staggered charge ordering, acting similarly to the n.n. electron-electron repulsion V. Therefore in varying V we keep constant the ratio $V/(g^2/K)$. For the sake of simplicity, we also keep a fixed J_2/J_1 ratio, although it is not the only possible choice.

Figure 2 reports typical phase diagrams at various temperatures as a function of the magnetic coupling $J = J_1S^2/t$ with $J_1 = J_2$ ($S = 3/2$) and of the repulsive e-e interaction $V = 0.5(g^2/K)$. At low temperature (left panel) there is a metallic (*i.e.* without charge-ordering) ferromagnetic phase (FM) when the charge-ordering (CO) terms V and g^2/K are not too large. This FM phase is naturally suppressed by the increase of the antiferromagnetic (AF) superexchange coupling J_1. When the charge mobility is suppressed by the CO terms, one finds two distinct possible phases. At low values of the AF coupling the pure CO effects dominate and a ferromagnetic (F) CO phase occurs at sufficiently large values of V (F-CO). The transition is first order, as found in reference [18], due to the exchange-correlation terms. On the other hand, by increasing the AF coupling, the CO ferromagnetism is destabilized and a CE phase takes place. This latter phase naturally realizes the best compromise between the electron mobility, favored by the ferromagnetic bonds, the CO, and the AF interactions increasing with J_1. The CE ordering arises due to competing lattice displacements. In particular a substantial shear mode is induced in the lattice to reconcile the (asymmetrical) JT deformations occurring in the Mn^{3+} ions with the (centrosymmetric) breathing deformations around the Mn^{4+} ions. The resulting lattice structure displays zig-zag chains formed by long bonds interlaced with zig-zag chains of short bonds. Then the peculiar CE magnetic structure naturally appears. In particular, according to Goodenough [9], orbital ordering makes the sign of the magnetic couplings to be correlated to the length of the bonds, with AF (F) magnetic couplings corresponding to short (long) bonds. Therefore, the lattice-driven chains with short bonds and with long bonds naturally translate into a lattice-driven CE magnetic structure.

The temperature evolution is represented in the three panels of Figure 2. By increasing T the weak ferromagnetism surviving in the CO phase at small J is rapidly suppressed in favor of a a CO paramagnetic phase. Also the CE region, being due to a delicate balance between CO, FM, and AF interactions, is reduced rather rapidly. The FM phase at small values of J_1 is instead based on the double-exchange mechanism, which is more robust and, upon increasing T, is only weakly "invaded" by the CO

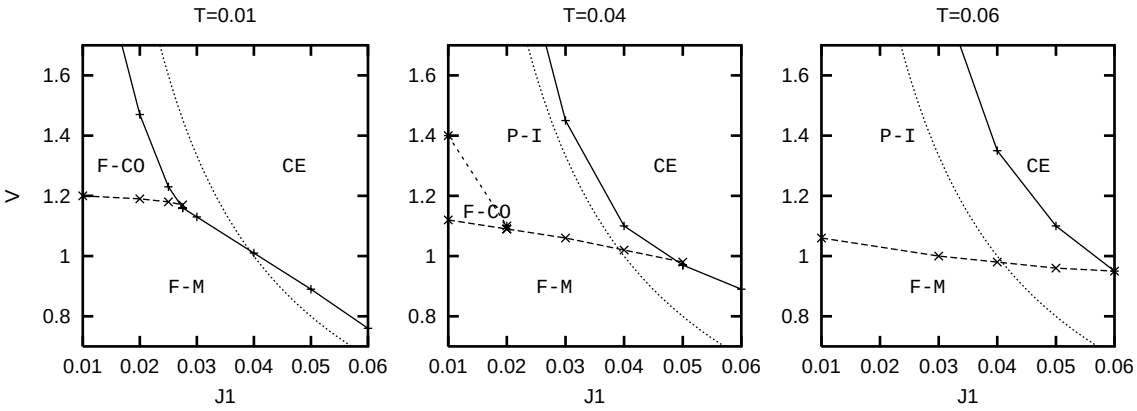

Fig. 2. Phase diagrams as function of the AF coupling J_1 and the electron-phonon or Coulomb parameter V, for different temperatures (see text).

paramagnetic phase. One also observes that compounds with a low-temperature CE magnetic structure, but laying near the CE-FM phase boundary, can undergo a first-order CE-to-FM transition upon increasing the temperature.

It is worth pointing out that, within our formal scheme, the CO paramagnetic phase is the only possible mean-field description of an insulating non-magnetic phase at moderate temperature values. The explored temperature range is indeed much too low to allow for a thermal disruption of the CO, which instead occurs at temperatures of the order of V. However, in strong coupling, one may speculate that a more refined description would allow for the disordering of the charge (possibly without spoiling the local lattice deformations around the charges) thus producing the disordered paramagnetic (and polaronic) phase which is observed in all manganites above a few hundreds of kelvins.

2.2 Sensitive role of the electronic bandwidth

A key issue is the role of the kinetic energy in the competition between the different phases. An extended experimental analysis of the phase diagrams of the various manganites [20,17] suggests that the electronic bandwidth, among other parameters such as lattice disorder, plays a primary role in determining the stability and the competition between the FM and the insulating phases. In our model we investigated this relevant point by varying the bare hopping amplitude in front of the double-exchange term in the Hamiltonian (1). We also assume that the same mechanism inducing the variation of the nearest neighbour hopping of the itinerant electrons in the e_g orbitals is responsible for variations of the hopping of the t_{2g} electrons as well. This affects the superexchange couplings J_1 and J_2, in particular J_1 is expected to arise from second-order hopping processes of the t_{2g} electrons $J_1 \propto t^2/U_{t_{2g}}$ (where $U_{t_{2g}}$ is some effective repulsion between electrons in the same doubly occupied t_{2g} orbital). According to this assumption, when the hopping t is increased without changing the intersite repulsion V one moves downwards in the phase diagrams of Figure 2, where the variable V/t is reported on the y-axis. At the same time, however, the increasing t produces an increase in the x-axis variable $J \propto t$. Therefore, by keeping all the Hamiltonian parameters fixed, but t and $J_1 = J_2$, one moves in the phase diagram along the dotted curves $V/t = A/J$ reported in Figure 2. These curves correspond to similar physical systems, where the only nearest neighbour electronic hopping amplitudes have been varied.

It immediately appears that systems which slightly differ by the electronic hopping amplitude can have different magnetic structures at low temperature (Fig. 2, left panel). In particular, by increasing t a first-order transition can occur at low temperature from a CE to a FM phase. Furthermore, the temperature evolution of systems with different bandwidth but laying near a phase boundary can be different. This is made apparent in Figure 3, where we report the temperature-magnetic field phase diagrams for three systems with different hopping (and therefore also different magnetic couplings J_1) laying on the same dotted curve $(V/t) = 0.04/J$. The three phase diagrams correspond to systems with slightly different magnetic couplings (differing at most by ten percent). Nevertheless, already at zero magnetic field, the three systems display a completely different evolution in temperature. The more insulating (*i.e.*, with smaller t) system having $J = 0.037$ (so that $(V/t) = 1.081$) never becomes metallic at zero field, but only undergoes a first-order transition from a low-temperature CE phase to a paramagnetic insulating phase at $T \simeq 0.032t$ (left panel, see also Figs. 4, 5). In the more metallic system (center panel) having $J = 0.038$ (and $V/t = 1.053$), the CE phase disappears at a lower temperature $T \simeq 0.02t$ and it is replaced by an intermediate FM phase. The ferromagnetic order and the metallicity is then destroyed at a higher temperature $T \simeq 0.032t$ where a paramagnetic CO phase takes place. We reiterate here that this latter phase is better to be intended as the mean-field representation of a disordered paramagnetic insulating phase. Finally, at even larger values of $J = 0.04$, corresponding to $V/t = 1$ the metallic phase is present already at low temperature and it survives up to a $T \simeq 0.05t$.

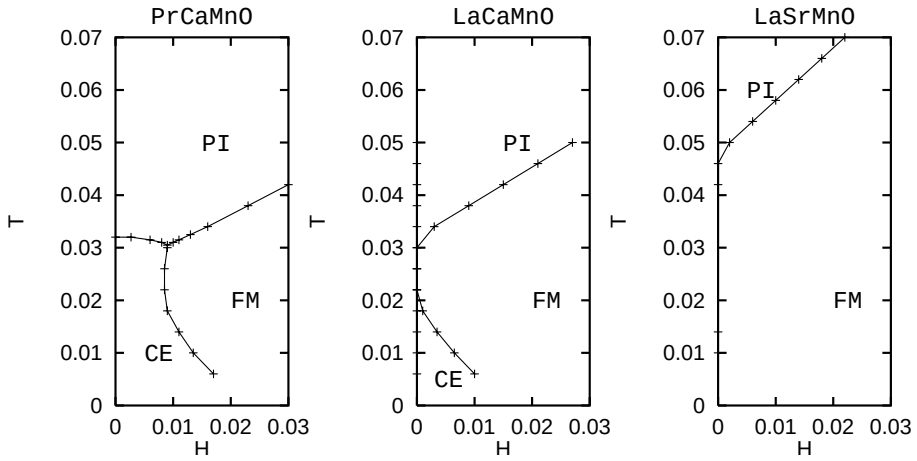

Fig. 3. Phase diagrams as function of temperature and magnetic field, for three typical bandwidth parameters (see text).

The relevant role of the kinetic energy in stabilizing the uniform metallic FM phase at the expenses of the CO phases and particularly of the one with CE magnetic order is made even more apparent in the presence of a magnetic field. This is particularly clear in the first panel of Figure 3, where the FM phase, which would be absent at zero field becomes the most stable solution at large enough H.

It is also worth mentioning that, due to the presence of screening, the metallic uniform solution is always a (local) minimum of the free energy. Therefore an (at least metastable) metallic solution is present even at zero field. The existence of a (local) minimum is a necessary condition for the occurrence of an hysteretic behavior at the transition. Of course the region of the hysteresis also depends on the height of the free energy barrier between the maxima, of domain walls and of other non-equilibrium properties. Nevertheless the region in T and H where two minima exist provides an (excess) estimate for the hysteresis region experimetally observed in half-doped $Pr_{0.5}Sr_{0.5}MnO_3$, $Nd_{0.5}Sr_{0.5}MnO_3$, $(Nd_{1-y}Sm_y)_{0.5}Sr_{0.5}MnO_3$ and $Pr_{0.5}Ca_{0.5}MnO_3$ [20,17].

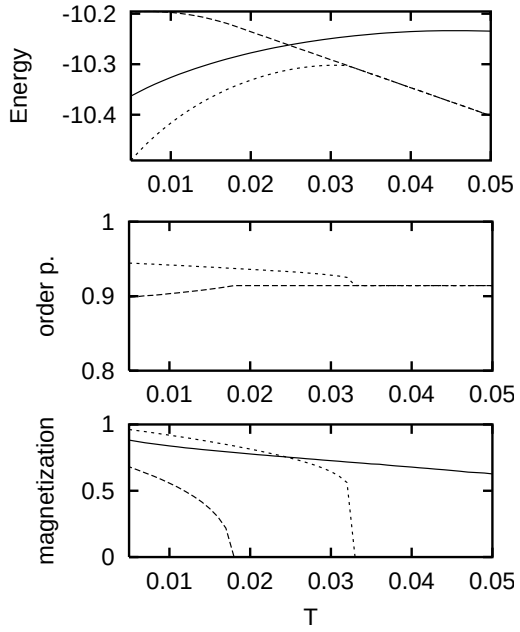

Fig. 4. Energy, order parameter (density) and magnetization *vs.* temperature at zero magnetic field. Full line: FM, dashed line: PI, dotted line: CE. The parameters correspond to the case PrCaMnO of Figure 3. In the CE phase, the magnetization is staggered.

2.3 Discussion

The previous subsection illustrated the main results of the present work:

i) The CE phase does arise in the present one-orbital model and is crucially related to competition between the JT and breathing distortions involved in the charge-ordered state on Mn^{3+} and Mn^{4+} sites respectively. The shear lattice deformation results from this competition and couples to the magnetic degree of freedom, merely through orbital ordering.

ii) Exchange-correlation corrections are essential to stabilize a metallic ferromagnetic phase, due to substantial screening of both Coulomb and electron-lattice interactions.

iii) The kinetic energy is a most effective parameter in determining the relative stability of the various phases upon varying the temperature and the magnetic field.

As far as point i) is concerned, in the present work we show that the CE phase not only arises from electronic mechanisms based on the presence of (at least) two orbitals per Mn site. The existence of a CE phase in a model *without* orbital degrees of freedom is quite remarkable. It is indeed repeatedly stated in the literature [12,13,21] that the CE phase is stabilized by the kinetic energy gain arising from the orbital ordering forming ferromagnetic chains. Our results are not in contrast with this viewpoint, but underline that the above purely electronic mechanism is not the only possible one, and that the coupling with lattice degrees of freedom can be of primary importance. In this regard our results are related to

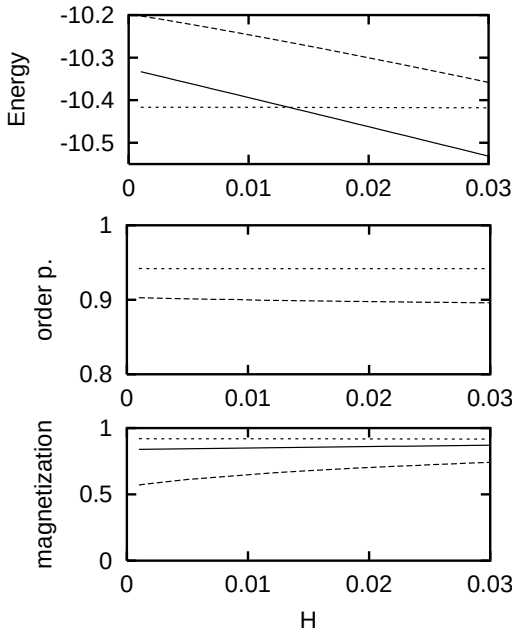

Fig. 5. Energy, order parameter (density) and magnetization *vs.* magnetic field at $T = 0.01$. Full line: FM, dashed line: PI, dotted line: CE. The parameters correspond to the case PrCaMnO of Figure 3. In the CE phase, the magnetization is staggered.

previous Hartree-Fock [14] and quantum Monte-Carlo [8] calculations, where the JT deformations were claimed to be relevant for the occurrence of a CE phase. Our low-temperature phase diagrams are qualitatively similar to the one reported in Figure 2c in reference [8] once the distinction between order and disorder in the orbital degrees of freedom is discarded [22]. Our contribution in this framework is to show that the lattice shear deformation is a relevant ingredient in its own even in the absence of cooperative mechanisms due to electronic or JT-induced orbital ordering.

Regarding point iii) we notice that a systematic analysis of the role of the hopping is relevant for the general understanding of the manganites. In the real materials of the general form $R_{1-x}A_xMnO_3$ (where R and A are trivalent rare earth and divalent alkaline earth ions respectively) the bandwidth can be varied by changing the radius of the perovskite A site (where the R and A ions are located). Depending on the averaged ionic radius the bond angle of Mn-O-Mn deviates from 180° in the orthorhombic lattice. The smaller the radius of the A site is, the larger is this angle, which reduces the Mn-O overlap and the effective Mn-Mn hopping. A systematic experimental analysis of this effect is reported in reference [17]. The results summarized in Figure 3 allow for a unified qualitative description of different half-doped materials. In particular the most insulating behavior in Figure 3a is consistent with the generic features of $Pr_{0.5}Ca_{0.5}MnO_3$. On the other hand, the center panel of Figure 3 shows the same qualitative behavior of $La_{0.5}Ca_{0.5}MnO_3$ or $(Nd_{1-y}Sm_y)_{0.5}Sr_{0.5}MnO_3$. Finally the most metallic system in the right panel is a good qualitative description of $La_{0.5}Sr_{0.5}MnO_3$. Nevertheless, it has been pointed out [23] that a rapid change in lattice constant K, rather than necessarily small changes of t, could be the clue for the very different behaviours of the systems $(A,A')_{0.5}MnO_3$. In our case this would correspond to an abrupt change along a vertical line in Figure 2, and would enhance the first-order character of the transitions.

A semi-quantitative agreement can even be reached. In fact, the pure double-exchange ferromagnetic critical temperature ($J/t = 0$) is, from our 2D mean-field calculation, $T_c \simeq 0.085t$. A 3D estimate enhances this value by a factor 3/2 owing to the number of nearest neighbours, yielding $T_c^{DE} \simeq 0.13t$. For an average value $t = 0.3$ eV one gets a transition temperature $\simeq 450$ K. It is reduced by the presence of the antiferromagnetic coupling, for instance in panel (c) of Figure 3, in zero field $T_c \simeq 0.05t$ thus $\simeq 270$ K in 3D, thus supporting De Gennes' simple mean-field picture. Then one obtains in the center panel the value $T_c^{CE} \simeq 180$ K, and in the left panel $T_c^{CE} \simeq 170$ K. These values are reasonable, as compared with experimental ones, in particular one notices that T_c^{CE} is strongly reduced compared to T_c^{DE}. This is due to the competition between the two order parameters (ferro and antiferro). Another way to understand it is to notice that in the CE phase the effective dimensionality is reduced by chain formation, together with charge localization this reduces the effective strength of double-exchange. On the other hand the effective antiferromagnetic exchange is close to that of stoechiometric $CaMnO_3$ with a T_c of 120 K.

We have also systematically investigated the role of the magnetic field in stabilizing the uniform FM phase. The typical energy differences involved in the first-order transitions are so small that accessible magnetic fields are sufficient to drive the transition from the insulating to the FM phases. Specifically, by taking a typical value of $t \simeq 0.3$ eV, one can see that $H/t = 0.015$ (where $H = g\mu_b SH$) roughly corresponds to ten teslas. This value agrees well with the typical values experimentally used to investigate the (T, H) dependence of the low-temperature CE insulating phase and the intermediate-temperature uniform FM phase [20,17].

3 Conclusion

Let us compare our approach with other models which have been proposed to describe the half-doping compounds. In our treatment, the main ingredient which is responsible for the CE-type magnetic ordering is the appearance of a shear deformation, with the consequent modification of the magnetic coupling along certain directions. In reference [8], two different orbitals are retained for the e_g electrons, but the shear deformation is absent. In their approach, the CE order arises because the orbitals prefer to have large overlaps along certain directions, thus favoring the kinetic energy along zig-zag chains where the spins are aligned ferromagnetically. In reference [13], the electron-lattice interaction is absent, and it is again the anisotropic e_g transfer amplitude of the two-orbital model which drives the CE state. In both cases,

however, the AF coupling $J \sim 0.1t$ necessary to achieve the CE state is one order of magnitude higher than what is estimated from experiments, signaling that there must be some additional effect contributing to the CE ordering. Finally, we reiterate that self-consistent screening is necessary to explain that phases with marked charge order come in very close competition with metallic phases. We believe that this is a crucial feature of doped manganites, that further models addressing coexistence and texturing of those phases at small scales must take into account.

References

1. For reviews see: *Colossal Magnetoresistance, Charge ordering, and Related Properties of Manganese Oxides*, edited by C.N.R. Rao, B. Raveau (World Scientific, Singapore, 1998); M. Imada, A. Fujimori, Y. Tokura, Rev. Mod. Phys. **70**, 1039 (1998); *Colossal Magnetoresistance Oxides*, in *Monographs in Cond. Matt. Science*, edited by Y. Tokura (Gordon and Breach, 1999).
2. D. Feinberg, P. Germain, M. Grilli, G. Seibold, Phys. Rev. B **57**, 5583 (1998); M. Capone, D. Feinberg, M. Grilli, Eur. Phys. J. B **17**, 103 (2000).
3. E.O. Wollan, W.C. Koehler, Phys. Rev. **100**, 545 (1955).
4. C. Zener, Phys. Rev. **82**, 403 (1951).
5. P.W. Anderson, H. Hasegawa, Phys. Rev. **100**, 675 (1955).
6. P.G. de Gennes, Phys. Rev. **118**, 141 (1960).
7. A.J. Millis, P.B. Littlewood, B.I. Shraiman, Phys. Rev. Lett. **74**, 5144 (1995).
8. S. Yunoki, T. Hotta, E. Dagotto, Phys. Rev. Lett. **84**, 3714 (2000).
9. J.B. Goodenough, Phys. Rev. **100**, 564 (1955).
10. S. Mori, C.H. Chen, S.-W. Cheong, Phys. Rev. Lett. **81**, 3972 (1998).
11. S.K. Mishra, R. Pandit, S. Satpathy, Phys. Rev. B **56**, 3184 (1997).
12. I.V. Solovyev, K. Terakura, Phys. Rev. B **83**, 2825 (1999).
13. G. Jackeli, N.B. Perkins, N.M. Plakida, Phys. Rev. B **62**, 372 (2000).
14. T. Mizokawa, A. Fujimori, Phys. Rev. B **56**, R493 (1997).
15. D.S. Dessau, Z.-X. Shen, in *Colossal Magnetoresistance Oxides*, in *Monographs in Cond. Matt. Science*, edited by Y. Tokura (Gordon and Breach, 1999).
16. J.H. Jung, K.H. Kim, D.J. Eom, T.W. Noh, E.J. Choi, J. Yu, Y.S. Kwon, Y. Chung, Phys. Rev. B **55**, 15489 (1997).
17. Y. Tokura, H. Kuwahara, Y. Moritomo, Y. Tomioka, A. Asamitsu, Phys. Rev. Lett. **76**, 3184 (1996).
18. L. Sheng, C.S. Ting, Phys. Rev. B **57**, 5265 (1998).
19. P.G. Radaelli, *et al.*, Phys. Rev. B **55**, 3015 (1997)
20. Y. Tokura, *et al.*, J. Appl. Phys. **79**, 5288 (1996).
21. S. Okamoto, S. Ishihara, S. Maekawa, Phys. Rev. B **61**, 14647 (2000).
22. Despite the qualitative resemblance of our phase diagrams with the one reported in reference [8], we also emphasize that our approach considers a strong local e-e repulsion. Possibly this major difference is responsible for the much lower values of the AF coupling J_1 in our results in comparison with the rather large values of $J_{\rm AF}$ in reference [8].
23. T. Egami, D. Louca, J. Supercond. **13**, 247 (2000).